DEPARTMENT OF PHYSICS
UNIVERSITY OF JYVÄSKYLÄ
RESEARCH REPORT No. 12/2016

DARK MATTER AND BARYOGENESIS IN HIGGS PORTAL MODELS

BY
VILLE VASKONEN

Academic Dissertation
for the Degree of
Doctor of Philosophy

To be presented, by permission of the
Faculty of Mathematics and Natural Sciences
of the University of Jyväskylä,
for public examination in Auditorium FYS1 of the
University of Jyväskylä on October 21st, 2016
at 12 o'clock noon

Jyväskylä, Finland
October 2016

ISBN 978-951-39-6744-4 (paper version)
ISBN 978-951-39-6745-1 (electronic version)
ISSN 0075-465X

Author Ville Vaskonen
Department of Physics
University of Jyväskylä
Jyväskylä, Finland

Supervisors Prof. Kimmo Kainulainen
Department of Physics
University of Jyväskylä
Jyväskylä, Finland

Dr. Kimmo Tuominen
Department of Physics
University of Helsinki
Helsinki, Finland

Reviewers Prof. Mark Hindmarsh
Department of Physics and Astronomy
University of Sussex
Brighton, United Kingdom

Prof. Kari Rummukainen
Department of Physics
University of Helsinki
Helsinki, Finland

Opponent Prof. James M. Cline
Department of Physics
McGill University
Montreal, Canada

Abstract

This work focuses on two of the main issues in current understanding of particle physics described by the Standard Model. The Standard Model, despite of its success, is not complete. Existence of dark matter has been clearly verified, but its nature is unknown. Also, the baryon asymmetry in the Universe hints that the Standard Model has to be extended. In this thesis we study Higgs portal models which both contain dark matter candidates, and can provide for a successful production of the baryon asymmetry.

Preface

The work contained in this thesis has been carried out during 2013-2016 at the Department of Physics, University of Jyväskylä, Finland. The financial support provided by the Finnish Cultural Foundation and the Magnus Ehrnrooth Foundation is gratefully acknowledged.

I would like to express my gratitude to Prof. Kimmo Kainulainen and Dr. Kimmo Tuominen for supervising my doctoral studies. I also wish to thank Dr. Tommi Alanne, Dr. Matti Heikinheimo, Dr. Sami Nurmi and Mr. Tommi Tenkanen with whom I have had a pleasure to work with. I thank my friends and the staff at the Department of Physics for a great working atmosphere. Big thanks to the Holvi collaboration and Atomin Pamaus.

Ville Vaskonen

List of Publications

This thesis is based on the work presented in the following publications:

[I] T. Alanne, K. Tuominen, and V. Vaskonen, *Strong phase transition, dark matter and vacuum stability from simple hidden sectors*, *Nucl. Phys.* **B889** (2014) 692–711, [arXiv:1407.0688].

[II] K. Kainulainen, K. Tuominen, and V. Vaskonen, *Self-interacting dark matter and cosmology of a light scalar mediator*, *Phys. Rev.* **D93** (2016), no. 1 015016, [arXiv:1507.04931].

[III] T. Alanne, K. Kainulainen, K. Tuominen, and V. Vaskonen, *Baryogenesis in the two doublet and inert singlet extension of the Standard Model*, *JCAP* **08** (2016) 057, [arXiv:1607.03303].

The author participated in writing of all articles, and performed the numerical analysis partially in publications [I, III] and completely in publication [II].

Contents

Chapter 1

Introduction

The Standard Model of particle physics (SM) describes elementary particles and their electromagnetic, weak and strong interactions. The electroweak sector unifying the electromagnetic and the weak forces was introduced by Sheldon Glashow, Steven Weinberg and Abdus Salam in 1960's [1–3]. The model initially includes four massless particles that carry the forces. The Higgs mechanism [4–7] then spontaneously breaks the $\mathrm{SU(2)_L} \times \mathrm{U(1)_Y}$ gauge symmetry leaving $\mathrm{U(1)_{EM}}$ as a manifest symmetry of the vacuum. The symmetry breaking gives masses to three gauge bosons, $W^{\pm}$ and Z, carrying the weak force. The photon, which carries the electromagnetic force, remains massless. The strong force mediated by massless gluons is described by quantum chromodynamics. In addition to the force carriers, the SM incorporates matter particles: three generations of quarks and leptons, and the Higgs boson, which is responsible for the symmetry breaking.

During the last 40 years the SM has been extensively tested in collider experiments. The $W^{\pm}$ and Z gauge bosons were observed at the LEP in 1983 [8, 9] and the heaviest SM fermion, the top quark, at the Tevatron in 1995 [10]. The final confirmation for the SM was the observation of the Higgs boson at the LHC in 2012 [11, 12]. The properties of the observed particles fit very well the SM predictions, and particles not belonging to the SM have not been found. Cosmological and astrophysical observations however hint that the SM is not the whole story of particle physics.

In 1929 Edwin Hubble discovered that the Universe is expanding [13]. Following this expansion backwards we find that at early stages of its evolution the Universe was very hot and dense. Due to expansion the Universe cooled, and finally when the temperature of the Universe dropped below 0.1 eV electrons combined with protons forming atoms during an epoch called recombination. Before recombination photons scattered frequently off free electrons, but as the density of free electrons greatly decreased in recombina-

tion the mean free path of photons increased. Briefly after recombination the mean free path of photons became greater than the horizon size and they were able to stream freely. These photons form the cosmic microwave background (CMB), which was first observed in 1964 [14].

Observations of temperature fluctuations in the CMB provide very important information about the state of the Universe. Recently the Planck space observatory [15], and its predecessor WMAP [16] have measured the basic parameters of the standard cosmological model, ΛCDM. The observations have shown that the visible (baryonic) matter, which SM describes, comprises only a small fraction, about 4.9%, of the total energy of the Universe today. Dark matter (DM), which interacts very weakly with the visible matter and was first observed in studies of movement of galaxies in galaxy clusters [17] and rotational curves of galaxies [18], accounts for 25.9% of the energy. The remaining 69.2% is dark energy, which causes accelerated expansion of the Universe. The nature of dark energy and DM is unknown.

Before recombination light nuclei were formed, when the temperature of the Universe was roughly 1 MeV, during the Big Bang Nucleosynthesis (BBN), introduced originally by Ralph Alpher and George Gamow in 1948 [19]. In the standard BBN scenario with three light neutrino flavours the abundances of light elements, namely deuterium, helium, and lithium, depend on neutron lifetime, which is known with good accuracy [20], and baryon-to-entropy ratio, which characterizes overabundance of baryons compared to antibaryons in the Universe.

Astrophysical evidences have shown that the visible matter is predominantly made of baryons, and the Universe can not consist of distinct regions of baryons and antibaryons [21]. This excess of baryons compared to antibaryons was produced before the BBN, but the actual details of producing the baryon asymmetry are not known.

The baryon-to-entropy ratio was first determined from abundances of light elements by comparing them to the standard BBN predictions. Later the CMB observations have given an independent and more accurate way of measuring the baryon-to-entropy ratio [15, 16]. Apart from the lithium problem, the baryon-to-entropy ratio measured from the CMB is in good agreement with the standard BBN predictions. The observed lithium abundance lies 4-5σ below the BBN prediction. This may be due to systematic uncertainties in astrophysical measurements and their interpretations, but may also require new physics.

Somewhere before the BBN the Universe experienced an inflationary epoch during which the Universe expanded rapidly. The inflationary era was originally introduced by Alan Guth in 1981 [22] to explain the uniformity of the CMB radiation and flatness of the Universe. Cosmic inflation can also

explain the origin of the large scale structure of the Universe. What exactly caused the cosmic inflation is not known. As a consequence of the inflationary era any baryon asymmetry existing before inflation gets diluted away. Hence, a dynamical mechanism for the baryon asymmetry production is needed.

In this thesis we will address the DM and the baryon asymmetry problems. These problems motivate our study of physics beyond the SM. The solution for the DM problem requires beyond SM physics as the SM does not include a DM particle. Physics beyond the SM is needed also to solve the baryon asymmetry problem, because all necessary ingredients for a successful dynamical baryon asymmetry production (or baryogenesis), known as Sakharov conditions [23], are not satisfied in the SM. We will concentrate on Higgs portal models, which form a very appealing class of models, providing DM candidates and sufficient conditions for baryogenesis, and have thus gained a lot of interest.

This thesis is organized as follows: First, in Chapter 2 we introduce particle DM and electroweak baryogenesis. We discuss both freeze-out and freeze-in mechanisms for dark matter production, and by describing details of electroweak baryogenesis we show why the SM has to be extended. Then, in Chapters 3, 4 and 5 we discuss the publications [I, II, III]: In Chapter 3 we study the simplest Higgs portal model, and show that these kind of models provide viable DM candidates and enable a strong first order electroweak phase transition, which is a prerequisite for electroweak baryogenesis. In Chapter 4 we consider fermionic DM studying also DM self-interactions, and in Chapter 5 we study electroweak baryogenesis in two-Higgs-doublet model extended with a real singlet scalar field. Finally in Chapter 6 we summarize our main results.

Chapter 2

Preliminaries

In this Chapter we will briefly introduce necessary ingredients needed in the following Chapters, where the publications [I, II, III] are discussed. We will first describe how the observed DM abundance can be produced in the early Universe. Then we will introduce electroweak baryogenesis, and discuss how the SM should be extended for successful production of the observed baryon-to-entropy ratio.

2.1 Particle dark matter

Most traditional DM candidates are new elementary particles, though also different possibilities, such as primordial black holes [24], have been considered. Here we will consider particle DM, for which there are two standard mechanisms for producing the observed abundance: freeze-out and freeze-in. We will next briefly explain these. Also different mechanisms exist, e.g. asymmetric DM [25].

The evolution of the number density, n_a, of DM particle a is governed by the Boltzmann equation

$$\dot{n}_a + 3Hn_a = \sum_j \int \mathrm{d}\Pi_a \mathrm{d}C_{a,j}, \tag{2.1}$$

where H is the Hubble parameter, which describes the expansion rate of the Universe, and the sum accounts for different processes which change the number of DM particles. In radiation dominated Universe

$$H = \sqrt{\frac{4\pi^3}{45} g_{\mathrm{eff}}(T)} \frac{T^2}{M_{\mathrm{Pl}}}, \tag{2.2}$$

where T is the temperature of the thermal bath[1], g_{eff} accounts for effective number of relativistic degrees of freedom in the bath and M_{Pl} is the Planck mass. The differential collision term $\mathrm{d}C_a$ for the process $a + a_1 + a_2 + \ldots \to b_1 + b_2 + \ldots$ is given by

$$\begin{aligned}\mathrm{d}C_a = &- \mathrm{d}\Pi_{a_1}\mathrm{d}\Pi_{a_2}\ldots\mathrm{d}\Pi_{b_1}\mathrm{d}\Pi_{b_2}\ldots \\ &\times (2\pi)^4\delta^4\left(p_a + p_{a_1} + p_{a_2}\ldots - p_{b_1} - p_{b_2}\ldots\right) \\ &\times \left(|M|^2_{a+a_1+\ldots\to b_1+b_2+\ldots} f_a f_{a_1}\ldots(1\pm f_{b_1})(1\pm f_{b_2})\ldots\right. \\ &\left. - |M|^2_{b_1+b_2+\ldots\to a+a_1+\ldots} f_{b_1} f_{b_2}\ldots(1\pm f_a)(1\pm f_{a_1})\ldots\right),\end{aligned} \tag{2.3}$$

where $|M|^2_{a+a_1+\ldots\to b_1+b_2+\ldots}$ and $|M|^2_{b_1+b_2+\ldots\to a+a_1+\ldots}$ are the squared amplitudes, averaged over the initial states and summed over the final states, of the process $a + a_1 + \ldots \to b_1 + b_2 + \ldots$ and its CP conjugate $b_1 + b_2 + \ldots \to a + a_1 + \ldots$, respectively, $+$ applies for bosons and $-$ for fermions, and

$$\mathrm{d}\Pi_k = \frac{g_k}{(2\pi)^3}\frac{\mathrm{d}^3 p_k}{2E_k}. \tag{2.4}$$

The number of intrinsic degrees of freedom of particle k is denoted by g_k, its momentum and energy by p_k and E_k, respectively, and its phase space distribution by f_k.

In the freeze-out scenario DM particles are in thermal equilibrium with the bath particles in the early Universe. When the scattering rate of DM particles with the bath particles becomes smaller than the Hubble rate, the DM number density freezes out from thermal equilibrium. After freeze-out the DM number density scales as the scale factor cubed, a^3.

For example, let us consider DM annihilation processes, where two DM particles annihilate to bath particles. In this case the Boltzmann equation reads[2]

$$\dot{n}_a + 3Hn_a = -\langle v\sigma_a\rangle\left(n_a^2 - (n_a^{\text{eq}})^2\right), \tag{2.5}$$

where

$$n_a^{\text{eq}} = \frac{g_a}{2\pi^2}m_a^2 T K_2(m_a/T) \tag{2.6}$$

is the thermal number density of DM particles and

$$\langle v\sigma_a\rangle = \frac{1}{8m_a^4 T K_2^2(m_a/T)}\int_{4m_a^2}^{\infty}\mathrm{d}s\,\sigma_a\,(s-4m_a^2)\sqrt{s}K_1(\sqrt{s}/T) \tag{2.7}$$

[1] In the standard cosmology the thermal bath, at least at temperatures below $T \sim 1\,\text{TeV}$, consists dominantly of SM particles. Alternative scenarios have also been considered; see e.g. Reference [26], where a non-standard thermal history producing the observed DM abundance in a Higgs portal model has been studied.

[2] This form of the Boltzmann equation is known as Zel'dovic-Okun-Pilkener-Lee-Weinberg equation [27, 28].

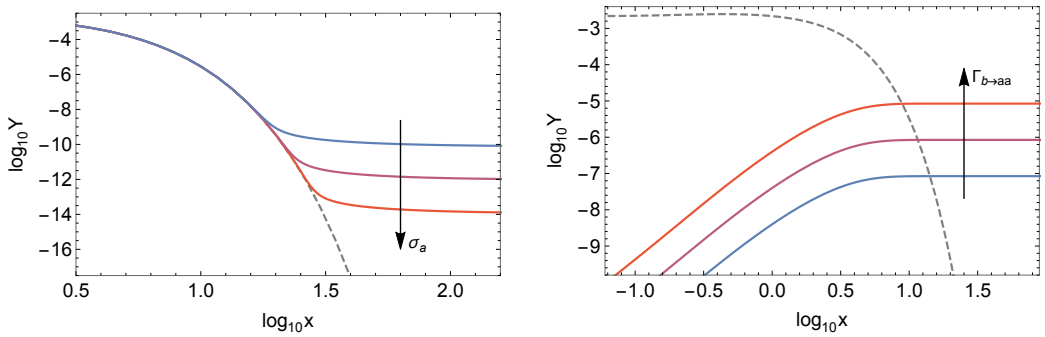

Figure 2.1: DM production via freeze-out (left panel) and freeze-in (right panel). Different solid lines from blue to red correspond to different interaction strengths between the DM and visible matter from weakest to strongest, respectively. The dashed line on the left panel shows the equilibrium abundance of the DM particle a, and on the right panel the equilibrium abundance of the particle b, which decays DM particles.

is the thermally averaged DM annihilation cross section [29]. Here K_j are the modified Bessel functions of the second kind, and σ_a is the DM annihilation cross section.

In the freeze-in scenario [30,31] the initial DM abundance is negligible, and the coupling between DM and the bath particles is so feeble, that DM never thermalizes with the bath. In this case DM is produced from the thermal bath by decays or annihilations of the bath particles. For example, if the bath particle b decays to two DM particles with decay width $\Gamma_{b\to aa}$, the Boltzmann equation reads

$$\dot{n}_a + 3Hn_a = 2\Gamma_{b\to aa} n_b^{\mathrm{eq}}. \tag{2.8}$$

As the temperature of the bath drops below m_b, the abundance of DM particles freezes, because the production of DM particles becomes very quickly negligible when the abundance of b particles in the thermal bath starts to drop exponentially following the thermal distribution. As opposed to the freeze-out scenario, in the freeze-in scenario the DM number density grows until it freezes.

Figure 2.1 depicts generic features of the freeze-out and freeze-in scenarios. The curves are obtained by solving numerically Equations (2.5) and (2.8) using dimensionless quantities Y_a and x defined as

$$Y_a = \frac{n_a}{s}, \quad x = \frac{m}{T}. \tag{2.9}$$

Here s is the entropy density,

$$s = \frac{2\pi^2}{45} h_{\text{eff}}(T) T^3, \tag{2.10}$$

where h_{eff} accounts for effective number of relativistic entropy degrees of freedom in the bath, and m is some mass scale related to the collision processes. In the freeze-out case we used $m = m_a$, and in the freeze-in case $m = m_b$. As Figure 2.1 illustrates, in the freeze-out case the larger the DM annihilation rate is the longer DM stays thermal, and the smaller the DM abundance finally is. In the freeze-in case the larger the production rate of DM particles is, the larger is the final DM abundance.

The DM abundance is given by

$$\Omega_a h^2 = \frac{h^2}{\rho_c} \rho_a(T_0) \approx 2.758 \times 10^8 \frac{m_a}{\text{GeV}} Y_a(T_0), \tag{2.11}$$

where the following the numerical values for the critical density and the CMB temperature today were used,

$$\rho_c = 8.098 \times 10^{-47}\,\text{GeV}^4 \times h^2, \quad T_0 = 2.348 \times 10^{-13}\,\text{GeV}. \tag{2.12}$$

According to the results from the Planck satellite [15] $\Omega_{\text{DM}} h^2 = 0.1198 \pm 0.0015$. Here h is the dimensionless Hubble parameter, related to the value of the Hubble parameter today via $H_0 = 100h$ (km/s)/Mpc.

2.2 Electroweak baryogenesis

The baryon asymmetry in the Universe is characterized by the baryon-to-entropy ratio η_B. The results from the Planck satellite [15] imply that $\eta_B = (8.7 \pm 0.3) \times 10^{-11}$. As discussed already in Chapter 1, a dynamical mechanism, called baryogenesis, producing the observed baryon-to-entropy ratio after cosmic inflation is needed. There are three necessary conditions for baryogenesis, known as the Sakharov conditions [23]:

1. violation of total baryon number B,

2. violation of charge conjugation (C) and charge-parity conjugation (CP) symmetries,

3. departure from thermal equilibrium.

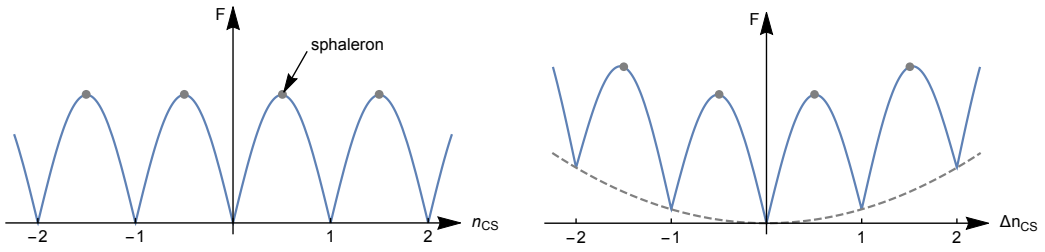

Figure 2.2: Illustrative plot of the gauge vacuum structure. F denotes the total free energy, and different gauge vacua are labelled by integer values of the Chern-Simmons number $n_{\rm CS}$. The configuration on top of the barrier is called a sphaleron. On the right panel $\Delta n_{\rm CS}$ measures the change in the Chern-Simmons number compared to the vacuum where $B = 0$.

The first condition is obvious, and needs no explanation. Second, the existence of baryon number violating process is not enough to produce baryon asymmetry, since the baryon number is odd under C and CP. If the C and CP symmetries are satisfied, the processes producing particles would have the same rate as their C and CP conjugate processes, that produce antiparticles. Hence, C and CP symmetries must be violated. The number densities of particles and antiparticles evolve in the thermal equilibrium similarly, since their masses are equal, so also departure from thermal equilibrium is required for baryon asymmetry production.

Electroweak baryogenesis (EWBG) is one of the most studied scenarios for producing baryon asymmetry in the early Universe [32]. In EWBG departure from equilibrium is provided by a first order phase transition, which breaks the electroweak symmetry. Scenarios of EWBG require new particles around the electroweak scale, as the SM does not fulfill all Sakharov conditions. This makes it also testable in collider experiments, and hence attractive. In the following we discuss details of the EWBG mechanism. We begin by describing how baryon number violation arises in the SM.

Due to the non-Abelian $\mathrm{SU}(2)_L$ symmetry, the gauge field vacuum structure in the electroweak sector is nontrivial with many degenerate minima separated by potential barriers, as illustrated in the left panel of Figure 2.2. Different minima are labeled by the Chern-Simmons number

$$n_{\rm CS} = \frac{g_L^2}{32\pi^2}\int \mathrm{d}^3x\epsilon^{ijk}\left(F^a_{ij}A^a_k - \frac{g_L}{3}\epsilon_{abc}A^a_iA^b_jA^c_k\right), \tag{2.13}$$

where g_L, A^a_μ and $F^a_{\mu\nu}$ are the $\mathrm{SU}(2)_L$ coupling constant, gauge field and field strength tensor, respectively. Transition from one minimum to a neighboring

minimum changes the Chern-Simmons number by one. At high temperatures these transitions can occur via classical thermal fluctuations [33].[3]

The anomalous $\mathrm{SU}(2)_L$ axial current results in non-conservation of total baryon and lepton number currents [34],

$$\partial_\mu j^\mu_B = \partial_\mu j^\mu_L = \frac{3g_L^2}{32\pi^2}\epsilon_{\mu\nu\alpha\beta}F^{a,\mu\nu}F^{a,\alpha\beta}. \tag{2.14}$$

Using the Chern-Simmons number, the change in the baryon and lepton numbers induced by the anomaly can be written as [35]

$$\Delta B = \Delta L = \int \mathrm{d}^4x \partial_\mu j^\mu_B = 3\Delta n_{\mathrm{CS}}. \tag{2.15}$$

Hence, transitions between different gauge vacua change the total baryon and lepton numbers. This fulfills the first Sakharov condition already in the SM.

Let us proceed by discussing the third Sakharov condition. In the early Universe the rate of electroweak processes, $\Gamma_{\mathrm{ew}} \sim \alpha^2 T \sim 10^{-3}T$, greatly exceeds the Hubble rate, $H \sim 10^{-18}T^2/\mathrm{GeV}$, thus thermal equilibrium is guaranteed. However, a first order electroweak phase transition (EWPT) illustrated in Figure 2.3 can momentarily provide for departure from thermal equilibrium. For a first order transition an essential feature is the existence of a potential barrier between the electroweak symmetric and electroweak breaking minima.

A first order EWPT proceeds by formation of bubbles of the electroweak broken phase, which expand and finally fill all of the Universe. Roughly, the inverse of the wall passage time is given by $\Gamma_w \sim v_w/l_w \sim 10^{-2}T$, where $v_w \sim 0.1$ is the bubble wall velocity and $l_w \sim 10/T$ is the width of the wall. At the bubble wall departure from thermal equilibrium is achieved, as the electroweak processes, which would maintain the thermal equilibrium, are slow compared to the inverse of the wall passage time. However, in the SM the EWPT is a crossover [36], thus new physics is needed to satisfy the third Sakharov condition.

It is not enough for a successful EWBG that the electroweak transition is of first order, but it also has to be sufficiently strong, This is generally characterized as

$$\frac{v_n}{T_n} > 1, \tag{2.16}$$

where T_n is the temperature at which the electroweak transition happens, and v_n is the value of the Higgs field at the electroweak breaking minimum

[3] Also transitions via quantum tunneling are in principle possible, but the tunneling rate is negligible, $\Gamma_{\mathrm{inst}} \propto e^{-8\pi^2/g_L^2} \sim 10^{-170}$.

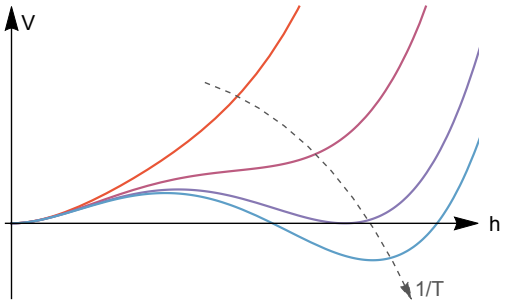

Figure 2.3: Illustration a first order EWPT. Shown is the evolution of the scalar potential from high temperatures (red), where the global minimum of the potential is electroweak symmetric ($h = 0$), to low temperatures (blue), where the Higgs field h obtains a non-zero vacuum expectation value, and the electroweak symmetry is broken.

at T_n. This is necessary in order to prevent baryon number wash-out in the electroweak breaking phase. Total baryon number increases the total free energy F as illustrated in the right panel of Figure 2.2, so actually the transitions between different gauge vacua, known as the sphaleron processes, tend to destroy any baryon excess. Hence, we must require that the rate of the sphaleron processes gets sufficiently slow inside the bubble.

The rate of the sphaleron processes in unit volume is in the electroweak symmetric phase given by [37]

$$\Gamma_{\rm sph}^{\rm sym} \approx 10^{-6} T^4, \tag{2.17}$$

and in the electroweak breaking phase [38]

$$\Gamma_{\rm sph}^{\rm br} = cT^4 e^{-E_{\rm sph}/T} \approx cT^4 e^{-40v(T)/T}, \tag{2.18}$$

where the prefactor c is a number of order one, $E_{\rm sph}$ is energy of the field configuration on top of the barrier, called a sphaleron, and $v(T)$ is the expectation value of the Higgs field. In the electroweak symmetric phase the sphaleron rate, $\tilde{\Gamma}_{\rm sph} = \Gamma_{\rm sph}/T^3$, is very fast compared to the Hubble rate, but drops in the electroweak broken phase quickly due to the exponential Boltzmann factor. If $v_n/T_n > 1$, the sphaleron rate at the bubble wall drops sufficiently fast below the Hubble rate, and baryon number will not be wiped out.

Existence of C and CP violating processes is vitally important for baryon number production. As discussed above, the sphaleron processes push the baryon number towards zero, but this is the situation only if C and CP are

conserved. Together C and CP violating processes can produce non-zero total left-chiral charge $Q_L = n_L - n_{\bar{L}} \neq 0$, but due to CPT invariance still $Q_L + Q_R = 0$. Since the sphaleron processes include only left-chiral fermions, this chiral asymmetry in the wall region effectively "tilts" the total free energy potential with respect to the one shown in the right panel of Figure 2.2, biasing sphaleron processes to convert the left-chiral charge to a non-zero baryon number, $B \neq 0$.

In the SM C-symmetry is maximally violated because of the chiral structure, but the only source for CP violation arises from the complex phase in the CKM quark mixing matrix [39, 40], which has been observed in decays of Kaons and B mesons [41]. It has been argued whether the CP violation in the SM is too weak to account for the observed baryon-to-entropy ratio [42–45]. Though there is no definite proof for that, it is quite generally agreed that a new source of CP violation is needed for a successful EWBG.

Chapter 3

Singlet scalar model

The idea of the Higgs mechanism is to introduce a scalar potential, which at the critical temperature gives a non-zero vacuum expectation value to the Higgs field ϕ, spontaneously breaking the $\mathrm{SU(2)_L} \times \mathrm{U(1)_Y}$ gauge symmetry down to $\mathrm{U(1)_{EM}}$. The scalar potential in the SM is given by

$$V(\phi) = \mu_\mathrm{h}^2 \phi^\dagger \phi + \lambda_\mathrm{h} (\phi^\dagger \phi)^2, \tag{3.1}$$

where $\lambda_\mathrm{h} > 0$ and $\mu_\mathrm{h}^2 < 0$.

New physics can couple to the Higgs field via terms of type $\lambda A \phi^\dagger \phi$. The operator A has to be SM singlet and, if one requires the theory to be renormalizable, its mass dimension less or equal to 2. Models where the new fields couple to the SM fields via this kind of operators are called Higgs portal models [46]. These models provide DM candidates and can modify the properties of the EWPT, and therefore have interesting consequences for cosmology and particle physics. Next we will study DM and EWPT in the simplest Higgs portal model.

3.1 Dark matter

Let us consider a Higgs portal model, where the portal sector includes only a real singlet scalar field s, which we assume to be Z_2 symmetric. Due to the Z_2 symmetry s in stable, and can thus act as a DM candidate. As this model is the simplest scalar extension of the SM which provides a dark matter candidate and modification to the EWPT, it has been studied extensively for example in References [31, 47–51].

The scalar potential of the model is

$$V(\phi, s) = \mu_\mathrm{h}^2 \phi^\dagger \phi + \lambda_\mathrm{h} (\phi^\dagger \phi)^2 + \frac{\lambda_\mathrm{hs}}{2} (\phi^\dagger \phi) s^2 + \frac{\mu_\mathrm{s}^2}{2} s^2 + \frac{\lambda_\mathrm{s}}{4} s^4. \tag{3.2}$$

To guarantee the stability of s, we assume that at the zero temperature vacuum the expectation value of the s field is zero.

Assuming that the portal coupling λ_{hs} is sufficiently large to bring s in thermal equilibrium with the SM bath, freeze-out of s number density determines the DM abundance. The annihilation cross section σ_{s} is given e.g. in Reference [50]. In Figure 3.1 the color coding shows the DM abundance relative to the observed abundance. If the s annihilation rate is small, the freeze-out occurs very early leaving too large DM abundance. This corresponds to the white region around $\lambda_{\mathrm{hs}} = 0$ in Figure 3.1.

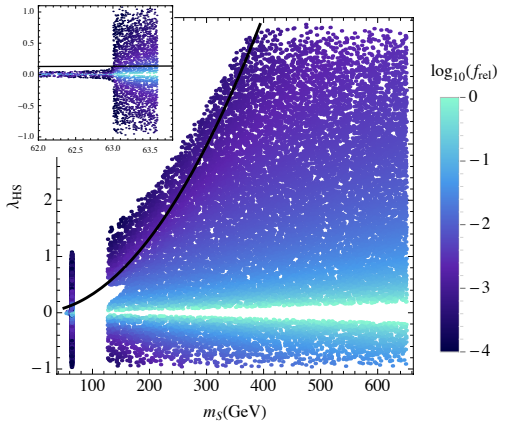

Figure 3.1: Singlet scalar DM: All points are compatible with the constraints from direct DM searches and LHC. Color coding shows the DM abundance relative to the observed abundance $f_{\mathrm{rel}} = \Omega_{\mathrm{s}}h^2/0.12$. A strong first order EWPT is possible only above the black line.

If the portal coupling is very small, $|\lambda_{\mathrm{hs}}| \lesssim 10^{-7}$, s never thermalizes with the SM bath. Then the DM abundance can be produced via the freeze-in mechanism. In reference [52] the freeze-in production has been studied and it has been shown that the Planck limit on isocurvature perturbations [53] gives strong constraints on portal sector couplings and masses in Higgs portal models.

There are various different attempts to observe DM particles via non-gravitational interactions. Direct DM searches aim on observing recoil effects as the DM particles scatter elastically off the target nuclei. These experiments have not yet observed DM, but they constrain the strength of the DM-nucleon scattering. For Higgs portal models, the current results from the LUX experiment [54] provide the most stringent constraints. In Figure 3.1

the region between the Higgs boson resonance, $m_s \sim m_h/2$, and $m_s \sim m_h$ is excluded by the LUX constraint.

If $m_s < m_h/2$, then the Higgs boson can decay to s. The Higgs decay width to non-SM particles is constrained by the LHC and Tevatron data [55–57]. Performing a χ^2 fit results a 2σ upper bound $\Gamma_{\text{inv}} < 1.0\,\text{MeV}$. This excludes large portal couplings below the Higgs resonance in Figure 3.1.

3.2 Electroweak phase transition

For a successful EWBG the EWPT has to be of first order and strong. In Chapter 5 we will describe a model where the EWBG can be successfully realized. Here we will only study properties of the EWPT in the singlet scalar extension of the SM.

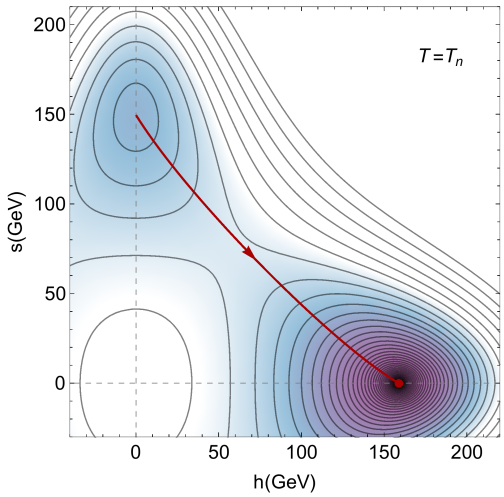

Figure 3.2: EWPT: The color shading indicates the depth of the potential and the contours show equipotentials. The red point shows the position of the global minimum at the nucleation temperature T_n, and the red line shows the path from the electroweak symmetric minimum to the electroweak broken minimum.

To study the properties of the EWPT, thermal corrections to the potential have to be taken into account. Figure 3.2 illustrates the phase transition pattern. At sufficiently high temperature the only minimum of the potential $V(h, s)$ is at $h = 0 = s$. The parameters of the potential can be chosen such that at some high temperature the s direction of the potential at $s = 0$ becomes unstable, and the global minimum of the potential is at $s \neq 0$.

Then, as the temperature decreases, the potential develops a minimum at $s = 0$, which breaks the electroweak symmetry. For the vacuum to break the electroweak symmetry, the electroweak broken minimum at $s = 0$ finally has to become deeper than the electroweak symmetric minimum at $s \neq 0$. When the transition to the electroweak broken minimum occurs, there has to be a bump in the potential between these minima for the phase transition to be of first order. For appropriate parameters, at some temperature below the critical temperature T_c at which the minima are degenerate, the potential energy difference between the electroweak symmetric and electroweak broken minima becomes sufficiently large compared to the height of the potential barrier between them, and the transition happens as shown in Figure 3.2.

Analytical conditions for a first order EWPT in this model have been derived in [58]. A necessary condition for the described symmetry breaking pattern is, that there exists a minimum at $s \neq 0$. This condition gives a lower limit on the portal coupling, $\lambda_{\mathrm{hs}} > 2m_{\mathrm{s}}^2/v^2$. The black line in Figure 3.1 shows this bound: a strong first order EWPT is possible only above that line. For that large portal coupling the freeze-out of s occurs so late that its abundance finally is at most $\sim 1\%$ of the observed DM abundance. We conclude that the singlet scalar extension of the SM enables a strong first order EWPT, but not simultaneously with the observed DM abundance. This result was first obtained in Reference [50].

3.3 Bubble formation

A crucial point for a successful first order EWPT is nucleation of bubbles of broken phase. Figure 3.3 shows the potential energy profile of a bubble as a function of the bubble radius. The potential energy gain in producing a bubble is proportional to the volume of the bubble, $\sim r^3$, whereas the energy loss due to the surface energy is proportional to the area of the surface of the bubble, $\sim r^2$. Qualitatively, if the bubble is too small the loss in the surface energy wins the gain in the potential energy, and the bubble shrinks. A bubble is said to be of critical size, if the sum of volume energy gain and surface energy loss is zero.

The bubble nucleation temperature T_n is defined as the temperature at which the probability of creating at least one bubble of critical size per horizon volume is of order one. The nucleation probability per unit time and volume for a bubble of critical size is given by [59]

$$\Gamma \sim T^4 \left(\frac{S_3(T)}{2\pi T}\right)^{3/2} \exp\left(-\frac{S_3(T)}{T}\right), \tag{3.3}$$

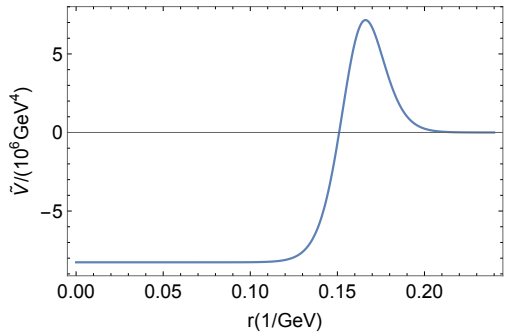

Figure 3.3: Bubble wall profile: The blue curve shows the potential energy corresponding to the path shown in Figure 3.2 as a function of the bubble radius.

where

$$S_3(T) = 4\pi \int r^2 \mathrm{d}r \left(\frac{1}{2} \left(\frac{\mathrm{d}h}{\mathrm{d}r} \right)^2 + \frac{1}{2} \left(\frac{\mathrm{d}s}{\mathrm{d}r} \right)^2 + \tilde{V}(h, s, T) \right), \tag{3.4}$$

is the three-dimensional Euclidean action for an O(3)-symmetric bubble corresponding to the path in the field space which minimizes the $S_3(T)$. Here $\tilde{V}(s, h, T)$ is the Z_2 symmetric scalar potential (3.2) including temperature corrections and normalized such that outside the bubble at $r \to \infty$ the potential energy is zero. The red line in Figure 3.2 shows the path which minimizes the action $S_3(T)$ and the potential energy along this path is shown in Figure 3.3.

If the thickness of the bubble wall is much smaller than the radius of the bubble, the action can be approximated as

$$S_3(T) = \frac{16\pi}{3} \frac{\sigma^3}{\delta V(T)^2}, \tag{3.5}$$

where $\sigma = \int \mathrm{d}\phi \sqrt{2V}$ is the surface tension integrated along the path minimizing the one dimensional action

$$S_1(T) = \int \mathrm{d}z \left(\frac{1}{2} \left(\frac{\mathrm{d}h}{\mathrm{d}z} \right)^2 + \frac{1}{2} \left(\frac{\mathrm{d}s}{\mathrm{d}z} \right)^2 + \tilde{V}(h, s, T) \right), \tag{3.6}$$

at $T = T_c$, and $\delta V(T)$ is the potential energy difference between the electroweak symmetric and broken minima. This is called the thin wall approximation.

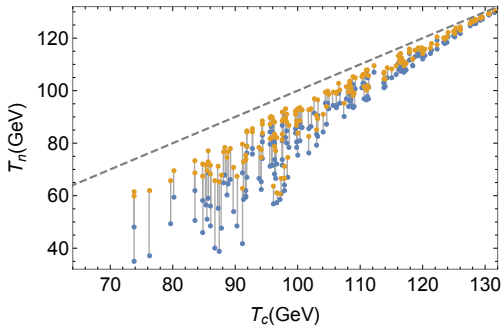

Figure 3.4: Bubble nucleation: Shown are the points which give a strong first order EWPT. Yellow points correspond to the a full calculation and yellow points to the thin wall approximation. Gray lines connect pairs corresponding to the same parameters. The dashed line corresponds to $T_n = T_c$.

Figure 3.4 shows the nucleation temperature for the points which give a strong first order EWPT. For comparison Figure 3.4 shows the nucleation temperature calculated by minimizing the full action (3.4) and by thin wall approximation. Though in the singlet scalar extension of the SM the minimization of the full three dimensional action is quite easy to implement numerically, studying also viability of the thin wall approximation is useful here, because in models where the scalar sector is more complicated the accurate calculation of the nucleation temperature is difficult. Form Figure 3.4 we see that the thin wall approximation does not work very well in these kind of scenarios.

Chapter 4

Fermionic dark matter

4.1 Dark matter and strong electroweak phase transition

In the previous chapter we showed, that in the simplest Higgs portal model it is not possible to simultaneously realize a strong first order EWPT and obtain the observed DM abundance, because for a first order EWPT the portal coupling λ_{hs} should be large, which inevitably leads to very small dark matter abundance, as the freeze-out of the DM candidate occurs too late. Hence, let us consider a Higgs portal model where the DM candidate is a singlet fermion ψ interacting with the SM particles via a singlet scalar s. In this model the dark matter abundance and the properties of the EWPT are determined by different couplings, so obtaining both a strong first order EWPT and the observed DM abundance simultaneously is possible.

The singlet fermion enters through the Lagrangian

$$\mathcal{L}_{\mathrm{DM}} = \bar{\psi}(i\partial\!\!\!/ - m)\psi + g_{\mathrm{s}} s \bar{\psi}\psi. \tag{4.1}$$

Since now s is not a DM candidate, we consider the general potential including also terms $\mu_{\mathrm{hs}}(\phi^\dagger\phi)s$, $\mu_1 s$ and $\mu_3 s^3/3$ in Equation (3.2). As the Higgs field gains a non-zero vacuum expectation value after the symmetry breaking, the mass eigenstates are linear combinations of the Higgs field h and the singlet scalar s,

$$H = h\cos\beta + s\sin\beta \quad S = -h\sin\beta + s\cos\beta. \tag{4.2}$$

The mixing modifies the couplings of the Higgs boson to other SM fields as compared to the SM; all couplings of H to SM particles are suppressed by $\cos\beta$. Modifications of Higgs boson couplings are constrained by the LHC results, which have shown that the couplings are very close to the SM

predictions. A χ^2 fit to the LHC and Tevatron data [55–57] gives an upper bound on the mixing, $\sin\beta < 0.45$, or equivalently $\cos\beta > 0.89$.

Similarly as in the model of singlet scalar DM discussed in Chapter 3, the freeze-out of ψ determines the DM abundance[1], and the interaction between the SM particles and ψ is constrained by the direct DM searches. In Figure 4.1 the color coding shows the DM abundance as a function of the $s\bar{\psi}\psi$ coupling $g_{\rm s}$ and the DM mass m_ψ.

The ψ freeze-out is dominated by the process $\bar{\psi}\psi \to SS$, which is proportional to the coupling $g_{\rm s}$. Hence the DM abundance can be fixed by choosing the $g_{\rm s}$ coupling. By choosing also the portal coupling $\lambda_{\rm hs}$ properly we can realize the symmetry breaking pattern described in Section 3.2 leading to a strong first order EWPT in this model simultaneously with the observed DM abundance. All points shown in Figure 4.1 give a strong first order EWPT.

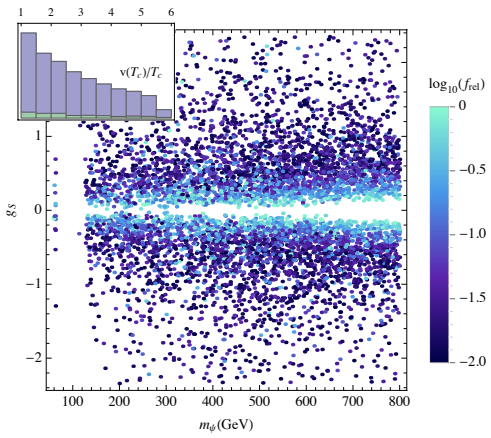

Figure 4.1: Singlet fermionic DM: The color coding shows the DM abundance $f_{\rm rel} = \Omega_\psi h^2/0.12$. All shown points give a strong first order EWPT, and the histogram shows the distribution of $v(T_c)/T_c$. The green portion of the bars correspond to $f_{\rm rel} > 0.5$.

4.2 Dark matter self-interactions

DM self-interactions provide a way test the viability of different DM models. The X-ray and gravitational lensing studies of galaxy cluster collisions reveal that after the collision the DM components of the clusters are not slowed

[1] Also DM freeze-in has been studied in a similar model [60].

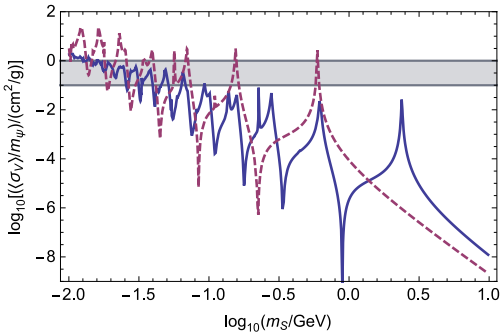

Figure 4.2: DM self-interaction cross section as a function of the mass of the mediator S for $g = 0.35$ and assuming the velocity $v_{\rm DM} = 10\,{\rm km/s}$. Solid and dashed lines correspond to $m_\psi = 400\,{\rm GeV}$ and $m_\psi = 100\,{\rm GeV}$, respectively. The gray region shows the region where the self-interaction is sufficiently strong to solve the problems associated to the small scale structure.

down as the gas components. These observations give an upper limit on the strength of DM self-interactions, $\sigma_{\rm DM}/m_{\rm DM} \lesssim 1{\rm cm}^2/{\rm g}$ [61–63].

There are also hints that the DM self-interactions may be quite strong. Sufficiently strong DM self-interactions would alleviate the tension between the observations and simulations on subgalactic scales. Simulations of collisionless cold DM show that the density profiles of galactic DM halos are cusped towards the center of the galaxy similar to the Navarro-Frenk-White density profile [64, 65],

$$\rho(r) \propto \frac{1}{(r/r_s)(1+r/r_s)^2}, \tag{4.3}$$

where r_s is a characteristic radius, whereas observations indicate flat cores of galactic DM halos [66, 67]. Also, recent observations of spatial offset of galactic DM halo from stars in Abell 3827 galaxy cluster can be interpreted as an evidence of sizeable DM self-interactions [68].

In the fermionic DM model, the S scalar, which mediates the interactions between DM and SM matter, also mediates the self-interactions of the DM particle ψ. The self-interaction cross section is proportional to $g_{\rm s}^4/m_{\rm S}^4$. To explain the small scale structure problems the strength of DM self-interactions should be $\sigma_{\rm DM}/m_{\rm DM} \simeq 0.1 - 1\,{\rm cm}^2/{\rm g}$ [63, 69, 70]. That large DM self-interaction cross section is usually quite difficult to obtain, and requires the mediator of the self-interactions to be light. Figure 4.2 shows σ_ψ/m_ψ as a function of $m_{\rm S}$. We see that $m_{\rm S} \lesssim 0.1\,{\rm GeV}$ can give sufficiently strong DM self-interaction if $m_\psi \sim 100\,{\rm GeV}$.

The resonant behavior of the blue and purple lines, showing the strength of

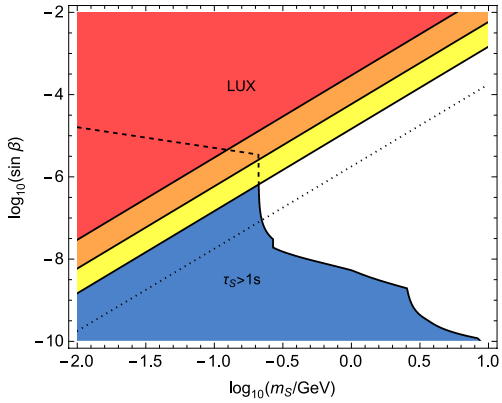

Figure 4.3: Constraints from BBN and LUX: Assuming that the mass of the DM particle ψ is within the LUX sensitivity, the red, orange and yellow regions are excluded by the direct DM searches for $g_\mathrm{s} = 0.4, 0.1, 0.02$, respectively. The dotted line indicates the expected XENON1T reach [75] for $g_\mathrm{s} = 0.4$. The blue region is excluded by the BBN.

the self-interactions in Figure 4.2, is due to Sommerfeld enhancement [71–74]: The Yukawa potential describing the interaction between DM particles ψ via S exchange has bound states at specific values of $g_\mathrm{s}^2 m_\psi / m_S$, which at low velocities enhance the scattering cross section compared to the leading order approximation. Similar enhancement affects in principle also DM freeze-out, but as the velocity of DM particles during freeze-out is very high, the Sommerfeld enhancement is negligible. During freeze-out the mean velocity of DM particles is $v_\mathrm{DM} \gtrsim 10^5\,\mathrm{km/s}$, whereas in the galactic halos $v_\mathrm{DM} \simeq 10 - 1000\,\mathrm{km/s}$ depending on the size of the galaxy. In Figure 4.2 the DM velocity is fixed to $v_\mathrm{DM} = 10\,\mathrm{km/s}$ corresponding to dwarf scale galaxies.

The cross section for DM scattering off nuclei is proportional to $g_\mathrm{s}^2 \sin^2\beta$. If $m_\mathrm{S} \ll m_\mathrm{H}$, then the S exchange dominates the dark matter-nucleon scattering, and the cross section is inversely proportional to m_S^4. In Figure 4.3 the red, orange and yellow regions show the LUX exclusion in the $(\sin\beta, m_\mathrm{S})$-plane for three different values of the $s\bar{\psi}\psi$ coupling strength g_s.

In the region where sizable DM self-interaction is obtained the lifetime of S is relatively long, as S can decay only to lightest SM fermions, and the scalar mixing angle has to be very small, $\sin\beta \lesssim 10^{-5}$, due to the LUX constraint. A successful BBN gives an upper limit on S lifetime. If S particles have not decayed to SM particles before the BBN begins at $T \simeq 4\,\mathrm{MeV}$, then their energy density would affect on expansion of the Universe, to which the BBN predictions of light elements abundances is very sensitive. To remain

within 2σ of the observed ^{4}He abundance, we require that the lifetime of S is less than one second. This excludes the blue region in Figure 4.3.

We see that there is some tension with the LUX and BBN limits in getting sufficiently strong DM self-interaction. The Sommerfeld enhancement can provide $\sigma_{\rm DM}/m_{\rm DM} \simeq 0.1 - 1\,{\rm cm}^2/{\rm g}$ consistently with the BBN and LUX bounds, but the window where this works is very narrow. This tension can be alleviated for example by introducing a new sterile neutrino, to which S can decay to, and which decays rapidly to SM neutrinos. This way the lifetime of S becomes very short, and sufficiently strong DM self-interaction can be obtained, since $m_{\rm S} \lesssim 0.1\,{\rm GeV}$ is allowed.

Chapter 5

Singlet scalar extended two-Higgs-doublet model

5.1 CP violation

In Chapter 3 we described a phase transition pattern in the singlet scalar extension of the SM, and showed that the model enables a strong first order EWPT. However, that model obviously does not provide a new source for CP violation. In two-Higgs-doublet model (2HDM), a new source for CP violation is provided. The scalar bosons in 2HDM are not necessarily CP eigenstates, because complex couplings in the scalar potential lead to mixing of neutral and imaginary parts of the doublets. The 2HDMs have been studied in connection to EWBG [76, 77] and in References [78, 79] it has been shown that the pure 2HDM is strictly constrained by observations.

We consider a singlet scalar extended two-Higgs-doublet model (2HDSM) described by the Lagrangian

$$\mathcal{L}_{\text{scalar}} = (D_\mu H_1)^2 + (D_\mu H_2)^2 + \frac{1}{2}(\partial_\mu S)^2 - V(H_1, H_2, S)\,, \tag{5.1}$$

where H_1 and H_2 are gauged $\mathrm{SU}(2)_L$ scalar doublets, D_μ is the gauge covariant derivative, S is a real singlet scalar field, and the scalar potential is given by

$$\begin{aligned} V(H_1, H_2, S) = &-m_1^2|H_1|^2 - m_2^2|H_2|^2 - \left(m_{12}^2 H_2^\dagger H_1 + \text{ h.c.}\right) - \frac{m_S^2}{2}S^2 \\ &+ \lambda_1|H_1|^4 + \lambda_2|H_2|^4 + \lambda_3|H_1|^2|H_2|^2 + \lambda_4(H_1^\dagger H_2)(H_2^\dagger H_1) \\ &+ \left(\lambda_5(H_2^\dagger H_1)^2 + \lambda_6|H_1|^2(H_2^\dagger H_1) + \lambda_7|H_2|^2(H_2^\dagger H_1) \;+\; \text{h.c.}\right) \\ &+ \frac{\lambda_S}{4}S^4 + \frac{\lambda_{S1}}{2}S^2|H_1|^2 + \frac{\lambda_{S2}}{2}S^2|H_2|^2 + \left(\frac{\lambda_{S12}}{2}S^2 H_2^\dagger H_1 + \text{ h.c.}\right). \end{aligned} \tag{5.2}$$

The singlet scalar enables for a strong first order EWPT and the two-Higgs-doublet sector gives a source for sufficient CP violation. We assume Z_2 symmetry for the S field, so that it can act as a DM candidate. Though here we have more freedom in the couplings, the observed DM abundance can not be obtained simultaneously with a first order EWPT [III] similarly as in the simple singlet scalar extension of the SM discussed in Chapter 3.

The spectrum of the model includes in addition to the Higgs boson, h_0, and the singlet scalar S, two neutral scalar bosons, H_0 and A_0, and charged scalar bosons, $H^\pm$. Collider experiments constrain the masses of these new scalars, as well as their mixing. For the S scalar similar constraints apply as in Chapter 3.

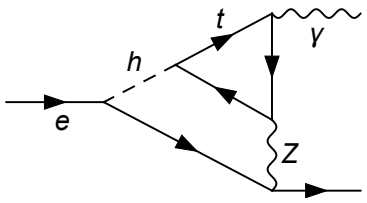

Figure 5.1: A diagram contributing to the electron EDM.

However, for baryogenesis, the most restrictive constraint arises from electric dipole moments (EDMs). The new scalar bosons which couple directly to the gauge bosons may increase the EDM of charged particles compared to the SM. Currently the most stringent bound for 2HDMs arises from electron EDM, d_e, for which the ACME experiment gives an upper limit $|d_e| < 8.7 \times 10^{-29}$ ecm [80]. The dominant conribution to d_e arises from two loop processes. The electron EDM in 2HDM can be written as

$$d_e = d_t^{h\gamma\gamma} + d_t^{hZ\gamma} + d_{W^\pm}^{h\gamma\gamma} + d_{W^\pm}^{hZ\gamma} + d_{H^\pm}^{h\gamma\gamma} + d_{H^\pm}^{hZ\gamma} + d^{H^\pm W^\mp \gamma}, \qquad (5.3)$$

where the upper indices refer to the particles which enter the effective vertex and the lower indices to the particle running in the loop. Here h stands for any neutral scalar from the two-Higgs-douplet sector, $h = h_0, H_0, A_0$. For example a diagram corresponding to the second term, $d_t^{hZ\gamma}$, is shown in Figure 5.1. The last term in (5.3) is slightly more complicated arising from various vertex and wave function corrections to the $H^\pm W^\mp \gamma$ vertex. The expressions for different contributions are given in Reference [81]. Figure 5.2 shows that large portion of otherwise viable parameter space is excluded by the electron EDM constraint.

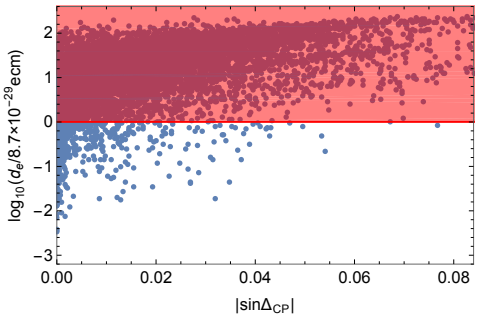

Figure 5.2: Constraints from electron electric dipole moment: Red region is excluded by the ACME constraint on electron EDM. All points correspond to otherwise viable parameter sets giving a strong first order EWPT.

5.2 Baryon asymmetry

The EWPT pattern is similar as described in Chapter 3, but here in the electroweak broken minimum both H_1 and H_2 obtain complex valued expectation values. The baryogenesis in the 2HDSM relies on spatially varying top quark mass over the bubble wall. To avoid unwanted flavor-changing neutral currents, we allow only one of the douplets to couple to fermions. We denote the doublet which couples to fermions by H_2. In the gauge $Z_\mu = 0$ (see [III] for details) the top quark mass is then given by

$$m_t(z) = \frac{y_t}{\sqrt{2}} h_2(z) e^{i\varphi_2(z)}. \tag{5.4}$$

where $\varphi_2(z)$ is the phase and $h_2(z)$ the magnitude of the neutral component of H_2.

We calculate the field configurations over the bubble wall by minimizing the one-dimensional Euclidean action,

$$S_1 = \int \mathrm{d}z \left(\sum_i \frac{(\partial_z h_i)^2}{2} + \frac{(\partial_z S)^2}{2} + \frac{h_1^2 h_2^2}{h_1^2 + h_2^2} \frac{(\partial_z \varphi)^2}{2} + V(h_i, S, \varphi) \right), \tag{5.5}$$

at the critical temperature. Here V is the scalar potential of the model for the neutral fields, which depends on the magnitudes of the neutral scalar fields, $h_{1,2}$, and the phase difference φ of the neutral components of H_1 and H_2. The use of one-dimensional action is justified here, since the bubbles are very large compared to the thickness of the wall; only a small number of expanding bubbles form within horizon, and they grow very quickly to fill the entire horizon. An example of the bubble wall profile is shown in Figure

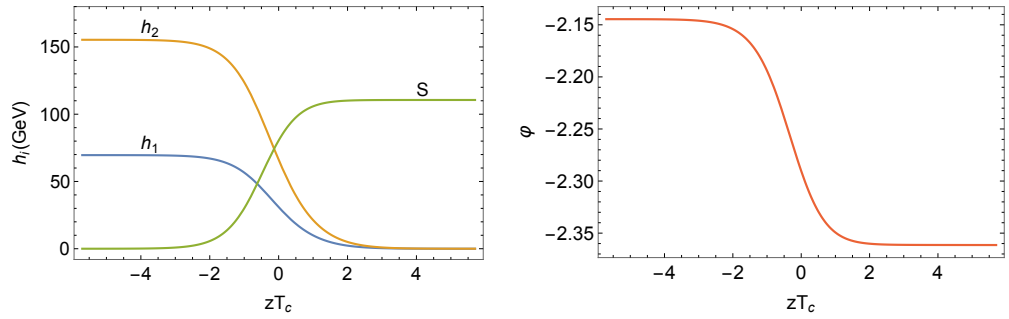

Figure 5.3: A representative example of the evolution of S, the magnitudes of the neutral scalar fields, $h_{1,2}$, and the phase difference φ of the neutral components of H_1 and H_2 fields over the bubble wall.

5.3. The z coordinate is chosen such that the bubble wall is around $z = 0$, and the electroweak broken phase is at $z < 0$.

To estimate the baryon asymmetry generated, we work in the thick wall limit, which assumes that the wavelength of the particles, $\lambda \sim 1/T$, is shorter than the thickness of the bubble wall, l_w. We have checked that indeed $l_w \gtrsim 3/T_c$.

The complex phase of the top quark mass results in a chiral force at the bubble wall, due to which particles and antiparticles are slowed differently (in the bubble wall frame). The effect of this force diffuses outside the wall producing a chiral asymmetry in front of the wall. To find out the chiral asymmetry which drives the baryon asymmetry production, we solve the chemical potentials $\mu_j(z)$, describing departure from the equilibrium particle densities, for top, anti-top and bottom from the transport equations given in References [82, 83]. From these we construct the left-chiral baryon chemical potential

$$\mu_{B_L} = \frac{1}{2}(1 + 4K_{1,t})\mu_t + \frac{1}{2}(1 + 4K_{1,b})\mu_b - 2K_{1,t_c}\mu_{t_c}, \tag{5.6}$$

where K_j are thermal averages defined in [82]. In the left panel of Figure 5.4 an example of the left-chiral baryon chemical potential is shown.

The left-chiral baryon chemical potential enters as a source term to the equation for baryon number violation rate [84],

$$\dot{n}_B = \frac{3}{2}\tilde{\Gamma}_{\text{sph}}\left(3\mu_{B_L}T^2 - \frac{15}{2}n_B\right). \tag{5.7}$$

The second term in the right-hand side in (5.7) describes baryon number relaxation by the sphaleron processes. Assuming that the bubble wall moves

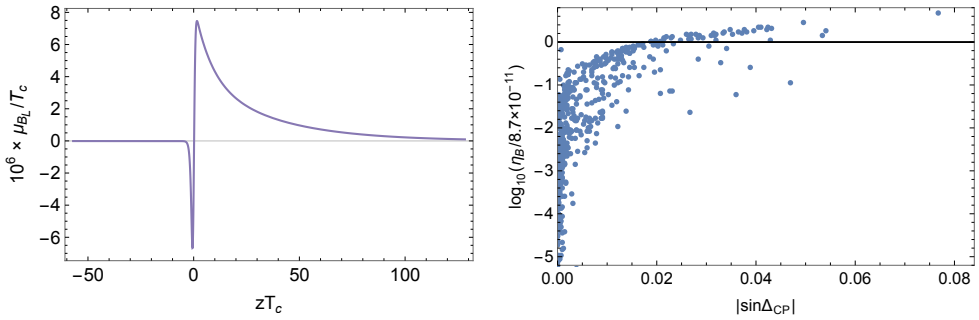

Figure 5.4: Left panel: A representative example of the left-chiral baryon chemical potential over the bubble wall. Right panel: Baryon-to-entropy ratio: Black line shows the observed value for η_B. All points are consistent with electron EDM and other constraints.

with constant velocity ξ_w, the baryon number n_B can be solved. Finally the baryon-to-entropy ratio, $\eta_B = n_B/s$, is given by

$$\eta_B = \frac{405}{4\pi^2 \xi_w g_{\rm eff} T_c} \int_0^\infty \mathrm{d}z\, \tilde{\Gamma}_{\rm sph}(z) \mu_{B_L}(z) e^{-45\tilde{\Gamma}_{\rm sph}(z) z/4\xi_w}. \tag{5.8}$$

We take $\xi_w = 0.1$ and $g_{\rm eff} = 106.75$. For the sphaleron rate we use a formula interpolating between the symmetric and the broken phase [78],

$$\tilde{\Gamma}_{\rm sph}(z) = \min(10^{-6} T_c, 2.4 T_c e^{-40 v(z)/T_c}), \tag{5.9}$$

where $v(z)^2 = h_1(z)^2 + h_2(z)^2$.

The right panel in Figure 5.4 shows the baryon-to-entropy ratio for the parameter sets which survive all constraints, including also the electron EDM bound. The horizontal axis, shown also in Figures 5.2, indicates how much the Higgs boson differs from a CP even state. Large η_B requires large CP violating angle $\sin\Delta_{\rm CP}$. Obtaining the observed baryon-to-entropy ratio is possible, though the electron EDM constraint excludes large portion of the potentially good parameter space.

5.3 The need for further analysis

We performed the baryon asymmetry calculation at the critical temperature T_c assuming that the bubble nucleation temperature T_n is not much lower than T_c. The left panel of Figure 5.5 indicates that the bubble nucleation actually occurs at quite significantly lower temperature than T_c, especially

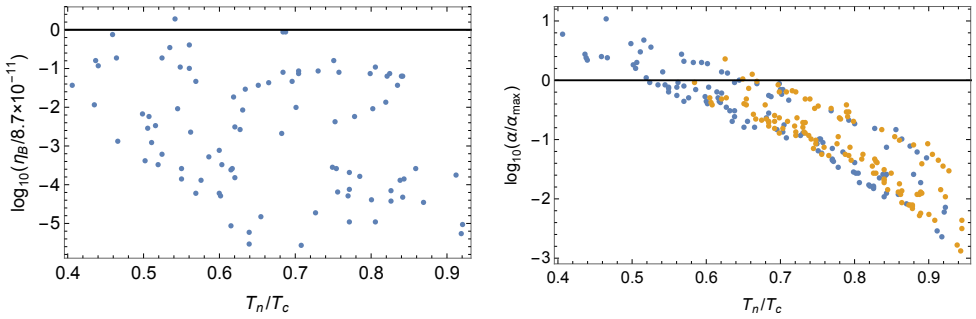

Figure 5.5: Left panel: Baryon-to-entropy ratio η_B as a function of the ratio of the nucleation and critical temperatures T_n/T_c. The nucleation temperature is calculated by thin wall approximation. Shown are the points from the right panel of Figure 5.4 for which the thin wall approximation gives a nucleation temperature. Right panel: Deflagration bound: only points below the line $\alpha/\alpha_{\max} = 1$ are allowed. For the yellow points the nucleation temperature is calculated using $T_n = T_c - 0.7(T_c - T_n^{\text{tw}})$.

for the points which give a large baryon-to-entropy ratio. The number of points in Figure 5.5 is smaller than in the right panel of Figure 5.4 because, according to the thin wall approximation, for many points the transition never occurs.

However, here we have used the thin wall approximation for the nucleation temperature, since the minimization of the full three-dimensional action is difficult in the 2HDSM. We found out in Chapter 3 that the thin wall approximation in these kind of models, where the barrier between the minima is due to a tree level term, underestimates the nucleation temperature. In some cases where the full calculation shows that the transition occurs, the thin wall approximation does not give any nucleation temperature. By analyzing the simple singlet scalar extension of the SM we have found that $(T_c - T_n)/(T_c - T_n^{\text{tw}}) < 0.7$, where T_n denotes the true nucleation temperature and T_n^{tw} the thin wall value. Still it seems that the assumption $T_n \approx T_c$ does not hold.

The calculation of baryon asymmetry also assumes that the bubble expansion is a subsonic deflagration, as required for efficient diffusion of particle asymmetries across the bubble wall. A necessary condition for deflagration is given by [85]

$$\alpha \equiv \frac{\Delta V(T_n)}{\rho(T_n)} < \frac{1}{3}(1 - \xi_w)^{-13/10} \equiv \alpha_{\max}\,, \tag{5.10}$$

where $\Delta V(T_n)$ is the potential energy difference from the electroweak sym-

metric minimum to the electroweak broken minimum, $\rho(T_n)$ is the radiation energy density in the broken phase and ξ_w is the bubble wall velocity. The right panel of Figure 5.5 shows that if the nucleation temperature is much smaller than the critical temperature, the expansion can not be deflagration. Taking into account the bias in the thin wall approximation, the expansion may remain subsonic, as indicated by the yellow points in the right panel of Figure 5.5.

To conclude, significant improvements are required to the analysis. Our calculations clearly indicate that a successful baryogenesis in the 2HDSM may be possible, but to make any definite conclusion the details of bubble nucleation and dynamics should be calculated carefully, and the baryon asymmetry calculation should be performed at the true bubble nucleation temperature.

Chapter 6

Summary

Cosmological and astrophysical observations indicate that there is physics beyond the SM. The SM does not provide a DM particle nor explanation for the baryon asymmetry in the Universe. In this thesis we have studied Higgs portal models, and shown that they provide viable DM candidates and strong first order EWPT as required for EWBG. In light of present experimental situation, the Higgs portal models provide a way to hide new physics in to hidden sectors only weakly coupled with the visible sector.

Starting from the simplest scalar extension of the Standard model, we described the production of the observed DM abundance, and the symmetry breaking pattern which leads to a first order EWPT. We found that in the simplest Z_2 symmetric scalar extension of the SM the DM abundance for the parameters which give a strong first order EWPT is at most a few percent of the observed DM abundance.

We then studied a model where the DM is a singlet fermion interacting with the SM particles via a real singlet scalar. We showed that in this model it is possible to simultaneously obtain the observed DM abundance with the singlet fermion, and a strong first order EWPT from the two-step symmetry breaking pattern provided by the singlet scalar.

We also studied DM self-interactions in the latter model, and tested the model against different experimental constraints from collider experiments and cosmological observations. We showed that self-interactions of the fermion mediated by the singlet scalar can be sufficiently strong to explain the small scale structure problems. However, there is some tension between the constraints from direct DM searches and BBN, as the singlet scalar is very long lived.

Finally we studied singlet scalar extension of the two-Higgs-doublet model, and found out that it can give rise to the observed baryon asymmetry in the Universe. We showed that the electron EDM bound constraints the parameter

space significantly, but it still does not exclude the whole parameter space giving sufficiently large CP violation for a successful EWBG. We also found that the analysis should be improved, because in these kind of models where the barrier between the electroweak symmetric and electroweak broken phases arises from tree level terms the bubble nucleation temperature tends to be much smaller than the critical temperature. Our analysis motivates further developments along these lines to investigate the viability of EWBG scenarios.

Bibliography

[1] S. L. Glashow, *Partial Symmetries of Weak Interactions*, *Nucl. Phys.* **22** (1961) 579–588.

[2] S. Weinberg, *A Model of Leptons*, *Phys. Rev. Lett.* **19** (1967) 1264–1266.

[3] A. Salam, *Weak and Electromagnetic Interactions*, *Conf. Proc.* **C680519** (1968) 367–377.

[4] F. Englert and R. Brout, *Broken Symmetry and the Mass of Gauge Vector Mesons*, *Phys. Rev. Lett.* **13** (1964) 321–323.

[5] P. W. Higgs, *Broken Symmetries and the Masses of Gauge Bosons*, *Phys. Rev. Lett.* **13** (1964) 508–509.

[6] G. S. Guralnik, C. R. Hagen, and T. W. B. Kibble, *Global Conservation Laws and Massless Particles*, *Phys. Rev. Lett.* **13** (1964) 585–587.

[7] T. W. B. Kibble, *Symmetry breaking in nonAbelian gauge theories*, *Phys. Rev.* **155** (1967) 1554–1561.

[8] **UA1** Collaboration, G. Arnison et al., *Experimental Observation of Isolated Large Transverse Energy Electrons with Associated Missing Energy at s**(1/2) = 540-GeV*, *Phys. Lett.* **B122** (1983) 103–116.

[9] **UA1** Collaboration, G. Arnison et al., *Experimental Observation of Lepton Pairs of Invariant Mass Around 95-GeV/c**2 at the CERN SPS Collider*, *Phys. Lett.* **B126** (1983) 398–410.

[10] **CDF** Collaboration, F. Abe et al., *Observation of top quark production in $\bar{p}p$ collisions*, *Phys. Rev. Lett.* **74** (1995) 2626–2631, [hep-ex/9503002].

[11] **ATLAS** Collaboration, G. Aad et al., *Observation of a new particle in the search for the Standard Model Higgs boson with the ATLAS detector at the LHC*, *Phys. Lett.* **B716** (2012) 1–29, [arXiv:1207.7214].

[12] **CMS** Collaboration, S. Chatrchyan et al., *Observation of a new boson at a mass of 125 GeV with the CMS experiment at the LHC*, *Phys. Lett.* **B716** (2012) 30–61, [arXiv:1207.7235].

[13] E. Hubble, *A relation between distance and radial velocity among extra-galactic nebulae*, *Proc. Nat. Acad. Sci.* **15** (1929) 168–173.

[14] A. A. Penzias and R. W. Wilson, *A Measurement of excess antenna temperature at 4080-Mc/s*, *Astrophys. J.* **142** (1965) 419–421.

[15] **Planck** Collaboration, P. A. R. Ade et al., *Planck 2015 results. XIII. Cosmological parameters*, arXiv:1502.01589.

[16] **WMAP** Collaboration, E. Komatsu et al., *Seven-Year Wilkinson Microwave Anisotropy Probe (WMAP) Observations: Cosmological Interpretation*, *Astrophys. J. Suppl.* **192** (2011) 18, [arXiv:1001.4538].

[17] F. Zwicky, *On the Masses of Nebulae and of Clusters of Nebulae*, *Astrophys. J.* **86** (1937) 217–246.

[18] V. C. Rubin and W. K. Ford, Jr., *Rotation of the Andromeda Nebula from a Spectroscopic Survey of Emission Regions*, *Astrophys. J.* **159** (1970) 379–403.

[19] R. A. Alpher, H. Bethe, and G. Gamow, *The origin of chemical elements*, *Phys. Rev.* **73** (1948) 803–804.

[20] **Particle Data Group** Collaboration, K. A. Olive et al., *Review of Particle Physics*, *Chin. Phys.* **C38** (2014) 090001.

[21] A. G. Cohen, A. De Rujula, and S. L. Glashow, *A Matter - antimatter universe?*, *Astrophys. J.* **495** (1998) 539–549, [astro-ph/9707087].

[22] A. H. Guth, *The Inflationary Universe: A Possible Solution to the Horizon and Flatness Problems*, *Phys. Rev.* **D23** (1981) 347–356.

[23] A. D. Sakharov, *Violation of CP Invariance, c Asymmetry, and Baryon Asymmetry of the Universe*, *Pisma Zh. Eksp. Teor. Fiz.* **5** (1967) 32–35.

[24] J. H. MacGibbon, *Can Planck-mass relics of evaporating black holes close the universe?*, *Nature* **329** (1987) 308–309.

[25] K. Petraki and R. R. Volkas, *Review of asymmetric dark matter*, *Int. J. Mod. Phys.* **A28** (2013) 1330028, [arXiv:1305.4939].

[26] T. Tenkanen and V. Vaskonen, *Reheating the Standard Model from a Hidden Sector*, arXiv:1606.00192.

[27] Y. B. Zel'dovich, L. B. Okun', and S. B. Pikel'ner, *Quarks: astrophysical and physicochemical aspects*, *Soviet Physics Uspekhi* **8** (1966), no. 5 702.

[28] B. W. Lee and S. Weinberg, *Cosmological Lower Bound on Heavy Neutrino Masses*, *Phys. Rev. Lett.* **39** (1977) 165–168.

[29] P. Gondolo and G. Gelmini, *Cosmic abundances of stable particles: Improved analysis*, *Nucl. Phys.* **B360** (1991) 145–179.

[30] L. J. Hall, K. Jedamzik, J. March-Russell, and S. M. West, *Freeze-In Production of FIMP Dark Matter*, *JHEP* **03** (2010) 080, [arXiv:0911.1120].

[31] J. McDonald, *Thermally generated gauge singlet scalars as selfinteracting dark matter*, *Phys. Rev. Lett.* **88** (2002) 091304, [hep-ph/0106249].

[32] A. G. Cohen, D. B. Kaplan, and A. E. Nelson, *Weak scale baryogenesis*, *Phys. Lett.* **B245** (1990) 561–564.

[33] V. A. Kuzmin, V. A. Rubakov, and M. E. Shaposhnikov, *On the Anomalous Electroweak Baryon Number Nonconservation in the Early Universe*, *Phys. Lett.* **B155** (1985) 36.

[34] G. 't Hooft, *Symmetry Breaking Through Bell-Jackiw Anomalies*, *Phys. Rev. Lett.* **37** (1976) 8–11.

[35] F. R. Klinkhamer and N. S. Manton, *A Saddle Point Solution in the Weinberg-Salam Theory*, *Phys. Rev.* **D30** (1984) 2212.

[36] K. Kajantie, M. Laine, K. Rummukainen, and M. E. Shaposhnikov, *Is there a hot electroweak phase transition at m(H) larger or equal to m(W)?*, *Phys. Rev. Lett.* **77** (1996) 2887–2890, [hep-ph/9605288].

[37] D. Bodeker, G. D. Moore, and K. Rummukainen, *Chern-Simons number diffusion and hard thermal loops on the lattice*, *Phys. Rev.* **D61** (2000) 056003, [hep-ph/9907545].

[38] P. B. Arnold and L. D. McLerran, *The Sphaleron Strikes Back*, *Phys. Rev.* **D37** (1988) 1020.

[39] N. Cabibbo, *Unitary Symmetry and Leptonic Decays*, *Phys. Rev. Lett.* **10** (1963) 531–533.

[40] M. Kobayashi and T. Maskawa, *CP Violation in the Renormalizable Theory of Weak Interaction*, *Prog. Theor. Phys.* **49** (1973) 652–657.

[41] J. H. Christenson, J. W. Cronin, V. L. Fitch, and R. Turlay, *Evidence for the 2 pi Decay of the k(2)0 Meson*, *Phys. Rev. Lett.* **13** (1964) 138–140.

[42] C. Jarlskog, *Commutator of the Quark Mass Matrices in the Standard Electroweak Model and a Measure of Maximal CP Violation*, *Phys. Rev. Lett.* **55** (1985) 1039.

[43] G. R. Farrar and M. E. Shaposhnikov, *Baryon asymmetry of the universe in the standard electroweak theory*, *Phys. Rev.* **D50** (1994) 774, [hep-ph/9305275].

[44] M. B. Gavela, P. Hernandez, J. Orloff, and O. Pene, *Standard model CP violation and baryon asymmetry*, *Mod. Phys. Lett.* **A9** (1994) 795–810, [hep-ph/9312215].

[45] T. Konstandin, T. Prokopec, and M. G. Schmidt, *Axial currents from CKM matrix CP violation and electroweak baryogenesis*, *Nucl. Phys.* **B679** (2004) 246–260, [hep-ph/0309291].

[46] B. Patt and F. Wilczek, *Higgs-field portal into hidden sectors*, hep-ph/0605188.

[47] V. Silveira and A. Zee, *Scalar phantoms*, *Phys. Lett.* **B161** (1985) 136–140.

[48] J. McDonald, *Gauge singlet scalars as cold dark matter*, *Phys. Rev.* **D50** (1994) 3637–3649, [hep-ph/0702143].

[49] C. P. Burgess, M. Pospelov, and T. ter Veldhuis, *The Minimal model of nonbaryonic dark matter: A Singlet scalar*, *Nucl. Phys.* **B619** (2001) 709–728, [hep-ph/0011335].

[50] J. M. Cline and K. Kainulainen, *Electroweak baryogenesis and dark matter from a singlet Higgs*, *JCAP* **1301** (2013) 012, [arXiv:1210.4196].

[51] J. M. Cline, K. Kainulainen, P. Scott, and C. Weniger, *Update on scalar singlet dark matter*, *Phys. Rev.* **D88** (2013) 055025, [arXiv:1306.4710]. [Erratum: Phys. Rev.D92,no.3,039906(2015)].

[52] K. Kainulainen, S. Nurmi, T. Tenkanen, K. Tuominen, and V. Vaskonen, *Isocurvature Constraints on Portal Couplings*, *JCAP* **1606** (2016), no. 06 022, [arXiv:1601.07733].

[53] **Planck** Collaboration, P. A. R. Ade et al., *Planck 2015 results. XX. Constraints on inflation*, arXiv:1502.02114.

[54] **LUX** Collaboration, D. S. Akerib et al., *First results from the LUX dark matter experiment at the Sanford Underground Research Facility*, *Phys. Rev. Lett.* **112** (2014) 091303, [arXiv:1310.8214].

[55] **ATLAS** Collaboration, G. Aad et al., *Measurements of the Higgs boson production and decay rates and coupling strengths using pp collision data at $\sqrt{s} = 7$ and 8 TeV in the ATLAS experiment*, *Eur. Phys. J.* **C76** (2016), no. 1 6, [arXiv:1507.04548].

[56] **CMS** Collaboration, V. Khachatryan et al., *Precise determination of the mass of the Higgs boson and tests of compatibility of its couplings with the standard model predictions using proton collisions at 7 and 8 TeV*, *Eur. Phys. J.* **C75** (2015), no. 5 212, [arXiv:1412.8662].

[57] **CDF, D0** Collaboration, T. Aaltonen et al., *Higgs Boson Studies at the Tevatron*, *Phys. Rev.* **D88** (2013), no. 5 052014, [arXiv:1303.6346].

[58] T. Tenkanen, K. Tuominen, and V. Vaskonen, *A Strong Electroweak Phase Transition from the Inflaton Field*, *JCAP* **1609** (2016), no. 09 037, [arXiv:1606.06063].

[59] A. D. Linde, *Decay of the False Vacuum at Finite Temperature*, *Nucl. Phys.* **B216** (1983) 421. [Erratum: Nucl. Phys.B223,544(1983)].

[60] M. Heikinheimo, T. Tenkanen, K. Tuominen, and V. Vaskonen, *Observational Constraints on Decoupled Hidden Sectors*, *Phys. Rev.* **D94** (2016), no. 6 063506, [arXiv:1604.02401].

[61] M. Markevitch, A. H. Gonzalez, D. Clowe, A. Vikhlinin, L. David, W. Forman, C. Jones, S. Murray, and W. Tucker, *Direct constraints on the dark matter self-interaction cross-section from the merging galaxy cluster 1E0657-56*, *Astrophys. J.* **606** (2004) 819–824, [astro-ph/0309303].

[62] S. W. Randall, M. Markevitch, D. Clowe, A. H. Gonzalez, and M. Bradac, *Constraints on the Self-Interaction Cross-Section of Dark Matter from Numerical Simulations of the Merging Galaxy Cluster 1E 0657-56*, *Astrophys. J.* **679** (2008) 1173–1180, [arXiv:0704.0261].

[63] A. H. G. Peter, M. Rocha, J. S. Bullock, and M. Kaplinghat, *Cosmological Simulations with Self-Interacting Dark Matter II: Halo Shapes vs. Observations*, *Mon. Not. Roy. Astron. Soc.* **430** (2013) 105, [arXiv:1208.3026].

[64] J. F. Navarro, C. S. Frenk, and S. D. M. White, *The Structure of cold dark matter halos*, *Astrophys. J.* **462** (1996) 563–575, [astro-ph/9508025].

[65] J. F. Navarro, C. S. Frenk, and S. D. M. White, *A Universal density profile from hierarchical clustering*, *Astrophys. J.* **490** (1997) 493–508, [astro-ph/9611107].

[66] B. Moore, *Evidence against dissipationless dark matter from observations of galaxy haloes*, *Nature* **370** (1994) 629.

[67] R. A. Flores and J. R. Primack, *Observational and theoretical constraints on singular dark matter halos*, *Astrophys. J.* **427** (1994) L1–4, [astro-ph/9402004].

[68] R. Massey et al., *The behaviour of dark matter associated with four bright cluster galaxies in the 10 kpc core of Abell 3827*, *Mon. Not. Roy. Astron. Soc.* **449** (2015), no. 4 3393–3406, [arXiv:1504.03388].

[69] M. Rocha, A. H. G. Peter, J. S. Bullock, M. Kaplinghat, S. Garrison-Kimmel, J. Onorbe, and L. A. Moustakas, *Cosmological Simulations with Self-Interacting Dark Matter I: Constant Density Cores and Substructure*, *Mon. Not. Roy. Astron. Soc.* **430** (2013) 81–104, [arXiv:1208.3025].

[70] J. Zavala, M. Vogelsberger, and M. G. Walker, *Constraining Self-Interacting Dark Matter with the Milky Way's dwarf spheroidals*, *Monthly Notices of the Royal Astronomical Society: Letters* **431** (2013) L20–L24, [arXiv:1211.6426].

[71] A. Sommerfeld, *Über die Beugung und Bremsung der Elektronen*, *Annalen der Physik* **403** (1931), no. 3 257–330.

[72] N. Arkani-Hamed, D. P. Finkbeiner, T. R. Slatyer, and N. Weiner, *A Theory of Dark Matter*, *Phys. Rev.* **D79** (2009) 015014, [arXiv:0810.0713].

[73] S. Cassel, *Sommerfeld factor for arbitrary partial wave processes*, *J. Phys.* **G37** (2010) 105009, [arXiv:0903.5307].

[74] S. Tulin, H.-B. Yu, and K. M. Zurek, *Resonant Dark Forces and Small Scale Structure*, *Phys. Rev. Lett.* **110** (2013), no. 11 111301, [arXiv:1210.0900].

[75] **XENON1T** Collaboration, E. Aprile, *The XENON1T Dark Matter Search Experiment*, *Springer Proc. Phys.* **148** (2013) 93–96, [arXiv:1206.6288].

[76] N. Turok and J. Zadrozny, *Phase transitions in the two doublet model*, *Nucl. Phys.* **B369** (1992) 729–742.

[77] J. M. Cline, K. Kainulainen, and A. P. Vischer, *Dynamics of two Higgs doublet CP violation and baryogenesis at the electroweak phase transition*, *Phys. Rev.* **D54** (1996) 2451–2472, [hep-ph/9506284].

[78] J. M. Cline, K. Kainulainen, and M. Trott, *Electroweak Baryogenesis in Two Higgs Doublet Models and B meson anomalies*, *JHEP* **11** (2011) 089, [arXiv:1107.3559].

[79] G. C. Dorsch, S. J. Huber, and J. M. No, *A strong electroweak phase transition in the 2HDM after LHC8*, *JHEP* **10** (2013) 029, [arXiv:1305.6610].

[80] **ACME** Collaboration, J. Baron et al., *Order of Magnitude Smaller Limit on the Electric Dipole Moment of the Electron*, *Science* **343** (2014) 269–272, [arXiv:1310.7534].

[81] T. Abe, J. Hisano, T. Kitahara, and K. Tobioka, *Gauge invariant Barr-Zee type contributions to fermionic EDMs in the two-Higgs doublet models*, *JHEP* **01** (2014) 106, [arXiv:1311.4704]. [Erratum: JHEP04,161(2016)].

[82] L. Fromme and S. J. Huber, *Top transport in electroweak baryogenesis*, *JHEP* **03** (2007) 049, [hep-ph/0604159].

[83] L. Fromme, S. J. Huber, and M. Seniuch, *Baryogenesis in the two-Higgs doublet model*, *JHEP* **11** (2006) 038, [hep-ph/0605242].

[84] J. M. Cline, M. Joyce, and K. Kainulainen, *Supersymmetric electroweak baryogenesis*, *JHEP* **07** (2000) 018, [hep-ph/0006119].

[85] J. R. Espinosa, T. Konstandin, J. M. No, and G. Servant, *Energy Budget of Cosmological First-order Phase Transitions*, *JCAP* **1006** (2010) 028, [arXiv:1004.4187].